

# **Improvements in Accuracy and Speed Using the Time-of-Transition Method and Dynamic Image Analysis For Particle Sizing**

## **Some Real-World Examples**

**B.B. Weiner<sup>1</sup>, Walther W. Tscharnuter<sup>1</sup> and N. Karasikov<sup>2</sup>**

<sup>1</sup>**Brookhaven Instruments Corporation, 750 Blue Point Road, Holtsville, NY 11742**

<sup>2</sup>**Galai Productions Ltd., Migdal Haemek, 10500 Israel**

The theory behind the particle sizing technique known as Time-of Transition is discussed in detail. Specifically, sources of error are enumerated and accounted for quantitatively. Improvements in the accuracy of measuring large, airborne particles is shown to be a result of increasing the speed of rotation and the deflection angle of the wedge prism as well as increasing the data acquisition rate. Several practical example of the technique are demonstrated as well as one example involving image analysis.

There are many techniques for measuring particle size, especially above one micron: sieves, optical microscopy, sedimentation, laser diffraction, electrical and optical zone counters. Each technique has its own advantages and disadvantages. The zone counters yield high resolution, but cannot be used with airborne particles or particles on a microscope slide. Diffraction instruments yield results quickly, simply and with good repeatability, but they suffer from low resolution. Instruments based on sedimentation yield good resolution and are accurate, but the measurement time is long with broad distributions. Microscopy yields important information about shape, but is relatively slow, especially for broad distributions. Sieves are very inexpensive, but yield low resolution size distribution information and require skill in their use and long-term maintenance.

A technique known as time-of-transition (TOT) was introduced a few years ago (1,2). It offers an interesting combination of advantages. Measurements are made on single particles, so the resolution is relatively high. Unlike the zone-counters, the size is not determined by the pulse height. Instead, the size is determined by the pulse width. Therefore, calibration is not required, and, to first order, the results are not dependent on the optical properties of the particle.

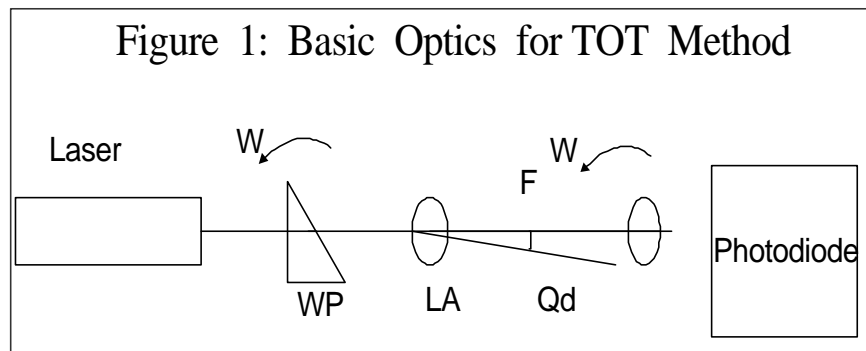
Early implementations of the TOT technique were relatively slow, for reasons explained in the theory section of this paper. As a result, the TOT technique did not find as many useful applications as it does today.

The purpose of this paper is to show the limitations as they exist today, discuss the improvements, and present some interesting data taken in the past few years.

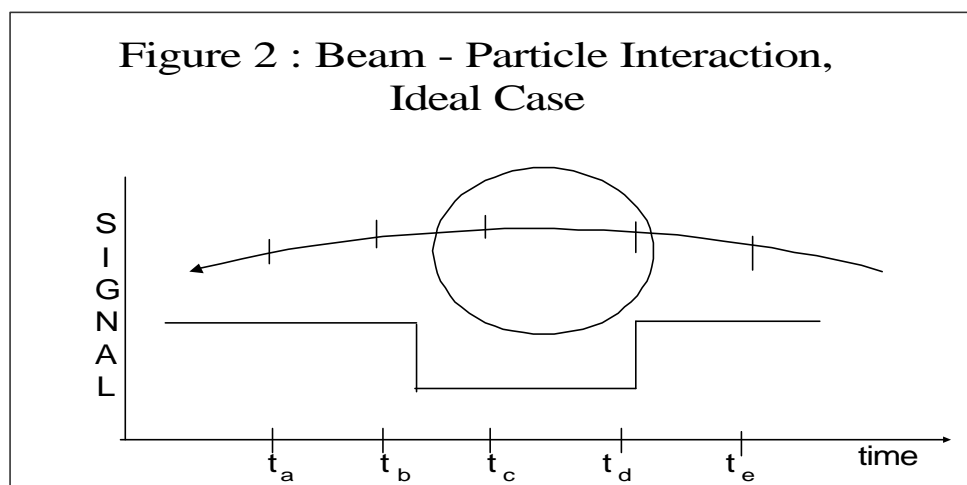
## Theory

**Fundamental Principle of TOT.** Figure 1 shows the basic optics. A collimated HeNe laser beam, wavelength  $\lambda = 632.8 \text{ nm}$ , passes through a wedge prism (WP) which causes the beam to deviate from the optical axis by the deflection angle  $\theta_d$ . The WP is made to rotate at an angular frequency  $\omega = 2\pi\nu$ . A lens (LA) focuses the beam down to a spot size ( $1/e^2$  diameter) of 1.2 microns using a lens of focal length  $F$ . The rotating, focused, deflected beam describes a circle of diameter  $D$  in space, where, for simplicity, it is assumed, for the moment, that

$D \gg d_p$ , the particle diameter. Particles are presented in a variety of ways to the beam: entrained in flowing or stirred liquid; on a raster-scanned microscope slide; entrained in flowing air; or simply sedimenting in air or liquid. A photodiode is placed directly behind the particles, perpendicular to the optical axis.



The signal on the photodiode is lower during the time the beam is crossing the particle. The ideal case is shown in Figure 2. By measuring the pulse width  $\Delta t$  and multiplying by the tangential velocity,  $V_T = \omega F \tan \theta_d$ , one obtains the distance the beam traveled across the particle. Equating this distance with the particle size makes the TOT technique one of the simplest available for calculating particle size from raw data.



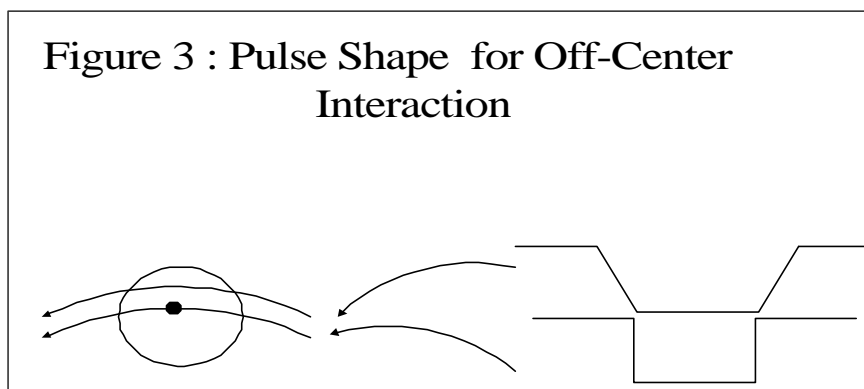
The technique is easily adaptable to different size ranges by changing the focal length, the deflection angle, and the rotational frequency. For the results described in this paper, two focal lengths  $F$  were used: 1.6 cm and 3.15 cm, corresponding to spot sizes of 1.2  $\mu\text{m}$  and 2.4  $\mu\text{m}$ , respectively. One version of the instrument, the Galai CIS-1, uses a rotational frequency of 80 Hz; a faster version, the Galai CIS-100, uses 200 Hz. Three deflection angles have been used:  $1^\circ$  or  $2^\circ$  with the CIS-1 and  $4^\circ$  with the CIS 100. The configurations and resulting  $V_T$  are summarized in Table I.

<b>Table I:</b> $q_d$	<u>CIS-1 (<math>\nu=80</math> Hz)</u>	<b>Tangential</b>	<b>Velocities</b>	
	$F = 1.6$ cm	$F = 3.15$ cm	<u>CIS-100 (<math>\nu=200</math> Hz)</u> $F = 1.6$ cm	$F = 3.15$ cm
$1^\circ$	0.140 $\mu\text{m}/\text{ms}$	0.276 $\mu\text{m}/\text{ms}$	-----	-----
$2^\circ$	0.281 $\mu\text{m}/\text{ms}$	0.553 $\mu\text{m}/\text{ms}$	-----	-----
$4^\circ$	-----	-----	1.41 $\mu\text{m}/\text{ms}$	2.77 $\mu\text{m}/\text{ms}$

The lower rotational frequency and smaller deflection angles of the CIS-1 make it difficult to measure accurately larger particles, especially ones sedimenting under gravity in air. They either move too fast or are not small compared to the circling diameter  $D$ . By using a  $4^\circ$  instead of a  $1^\circ$  or  $2^\circ$  deflection angle, by increasing the rotational frequency from 80 Hz to 200 Hz, and by increasing the data rate from 1 MHz to 10 MHz one can now make measurements that are an order of magnitude faster. Thus, large particles from dry powders can now be measured in air, although for large and dense particles, one is still limited to either suspending the particles in a flowing liquid or presentation on a moving microscope slide covered with a sparse, random layer of the dry particles.

In practice, there are potential errors in applying this technique. Each is described below along with the method used to correct or compensate for the errors involved.

**Off-Center Interactions: Chords.** Figure 3 shows a typical off-center interaction between the circling beam and the particle: the beam transits across a chord. If such a pulse were allowed, the resulting size distribution would be broadened and shifted to smaller average sizes.



The pulse shapes for a transit across a diameter and across a chord are also shown in Figure 3. Note the faster rise and fall times (higher absolute slopes) for the transit across the diameter. In the ideal case the minimum rise/fall time is set by the spot size and  $V_T$ . Pulses with rise/fall times greater than a few times the minimum are rejected and do not effect the resulting size distribution.

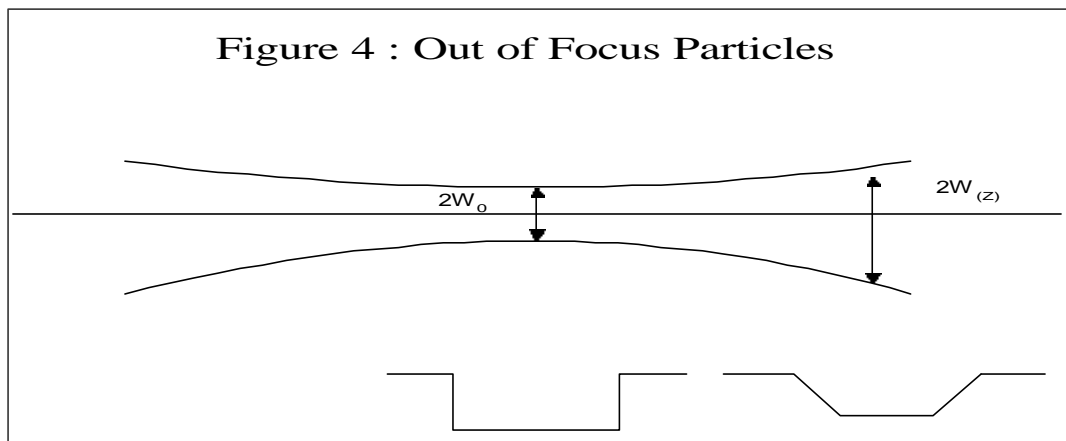
If the criterion is too strict, many transit crossings are rejected and the statistical error is high; however, the distribution width is more accurate, allowing good resolution of multiple peak distributions. If the criterion is too lenient, the statistical error is low; however, the distribution is artificially broadened, lowering the resolution.

By default the criterion is set such that the standard deviation of the distribution of a monodisperse sample is about  $\pm 17\%$ . An alternate setting yields  $\pm 10\%$ , although the experiment duration increases. These values place a practical limit on the resolution of the instrument. Electro- and optical zone counters as well as field-flow fractionation devices offer higher resolution, some capable of resolving peaks just a few percent apart. However, compared to Fraunhofer diffraction devices, the resolution offered by the TOT method is much higher.

To test the limits of the theory, the criterion for rejecting chords was set very tight, resulting in a measured standard deviation from a monodisperse sample of  $\pm 2.5\%$ . This shows the ultimate capability for resolving peaks is quite high, though not necessary in many practical cases of interest.

**Out of Focus Particles.** Figure 4 shows an expanded view of the focused beam. The radius  $w_0$  of the beam at the waist is  $0.6 \mu$  (when  $F = 1.6 \text{ cm}$ ), and the radius  $w(z)$  a distance  $z$  away is given (3) by:

$$w(z) = w_0 \cdot \sqrt{\left(1 + \left(\frac{\mathbf{I} \cdot z}{\mathbf{p} \cdot w_0^2}\right)^2\right)}$$



When a particle is out of focus it appears larger with a blurred boundary. In addition, the intensity per unit area of the beam is less than it is at the waist. The resulting pulses, one due to a transit at the waist and one due to a transit at  $w(z)$ , are also shown.

The pulse associated with transit at  $w(z)$  has a smaller amplitude, a greater width, and a longer rise/fall time than for a pulse associated with a transit at the

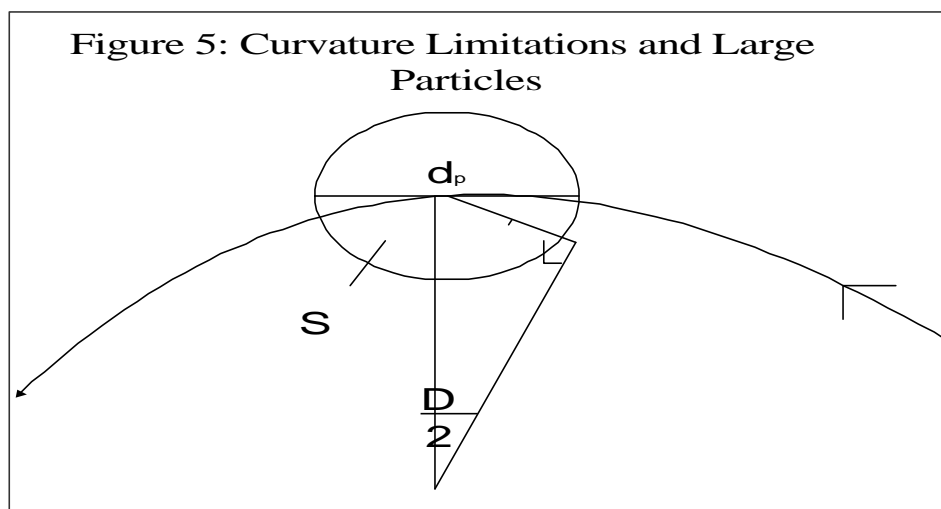
waist. If the rise/fall times are not equal and sufficiently short, the pulse is rejected as coming from a chord. In addition, by comparing the pulse width with the normalized pulse amplitude, one gets an additional rejection criterion. Specifically, an otherwise acceptable pulse is rejected unless it passes the normalized amplitude criterion. In this way it is possible to reject out of focus particles.

**Beam Diameter and Small Particle Limitation.** When the focused beam diameter ( $1.2\mu$

$F = 1.6 \text{ cm}$ ) is no longer small compared to the particle size, the pulse shape is no longer ideal: the leading and trailing edges are rounded. Since the beam has a Gaussian profile ( $TEM_{00}$ ), it is not difficult to deconvolute the measured pulse to produce a pulse corresponding to the particle size only. From this deconvoluted pulse the size is determined. In this way particles as small as  $0.5 \mu$  have been determined with good agreement. For presentation purposes only, the results may be extrapolated to  $0.1 \mu$ . By decreasing the wavelength and spot size, one could, in principle, make measurements down to approximately  $0.3\mu$ . The lower practical limit is set by the divergence of the beam, and for the current configurations, using a HeNe laser, this is  $0.5 \mu$

The accuracy of the size obtained from the deconvolution, especially for particles less than about  $10 \mu$ , depends on the accuracy with which the focused beam diameter is known. For this reason, the optics must be kept clean; otherwise, the spot size increases and the resulting particle sizes are overestimated. In critical cases, in this lower size range, use of a good quality quartz cell reduces the spot size to its theoretical limit compared to a slightly larger spot induced by the optical quality of some inexpensive, common, plastic cells. The repeatability and resolution, however, are not affected. If they are the primary concern, then a disposable plastic cell is preferred.

**Circling Beam Diameter and Large Particles.** The diameter of the circling beam is given by  $D = 2 F \tan \alpha_d$ . With  $\alpha_d = 4^\circ$  and  $F = 3.15 \text{ cm}$ ,  $D$  is  $4.4 \text{ mm}$ . As long as the particle diameter  $d_p$  is much smaller than  $D$ , the curvature of the circle as it transits across the particle can be ignored. Figure 5 shows the true path of a beam when  $D$  is not very much greater than  $d_p$ .



The arc  $S$  is always greater than the particle diameter  $d_p$ . The pulse width yields the arc length, not the particle diameter. The relationship between the two is

$$d_p / D = \sin (S / D)$$

This equation is used to correct for the difference. In the worst case ( $q_d = 4^\circ$ ,  $F = 3.15$  cm,  $d_p = 3,600\mu$ ), the arc  $S$  is 17% larger than  $d_p$ . For all other configurations the difference is smaller and in all cases easy to compensate. In the most common configurations, the correction amounts to less than a few percent.

**Particle Motion.** Figure 6 shows four positions on the circling beam at which a particle moving with a velocity  $V_\perp$  perpendicular to the optical axis might interact. The measured pulse width in all four cases corresponds to some distance  $x$  that is related to the actual particle diameter  $d_p$ .

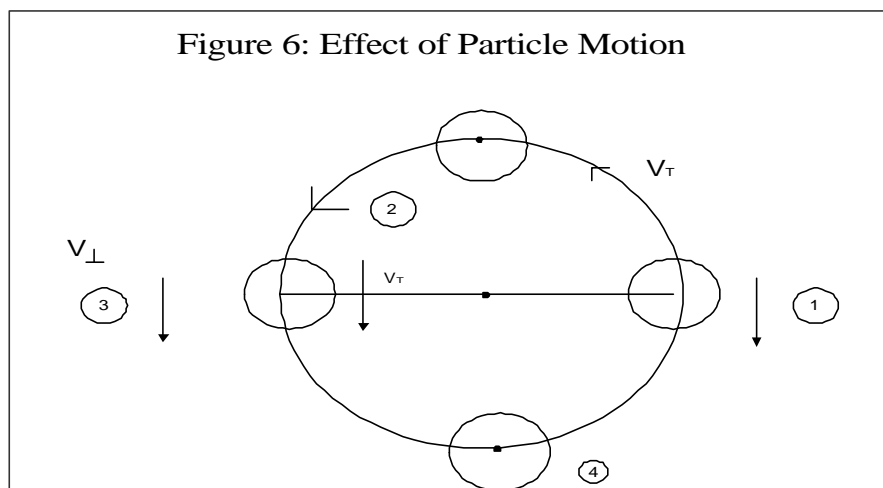
The apparent speed of the beam,  $V_R$ , is obtained from the vector sum of the tangential velocity and  $V_\perp$ . It is given by:

$$V_R = V_T \cdot \sqrt{\left(1 + \frac{1}{R^2} - \frac{2 \cos q}{R}\right)}$$

where  $R \equiv V_T / V_\perp$  and  $q$  is the angle from the x-axis to the center of the particle. The apparent size of the particle  $x = \Delta t V_R$ ; whereas, the particle diameter is  $d_p = \Delta t V_T$ . Assuming the beam and particle are equally likely to interact at any position over  $2\pi$  radians, the above equation can be integrated with the following results:

$$\bar{x} \cong d_p \cdot \left(1 + \frac{1}{R^2}\right)^{1/2} \qquad \frac{s}{\bar{x}} \cong \frac{1}{2R \left(1 + \frac{1}{R^2}\right)}$$

where  $\bar{x}$  is the mean and  $s / (\bar{x})$  is the relative standard deviation. As long as the flow velocity is set to 1/5th or less of the tangential velocity ( $R \geq 5$ ), the mean is within 2% of the true diameter, and the relative std. dev. is 10% or less. Given the 10-fold increase in tangential velocity of the CIS-100 over the CIS-1, a greater range of samples can now be measured accurately.



**Concentration Limitations.** The lower limit of detection is one particle. For this reason, the TOT method is capable of measuring much lower concentrations than Fraunhofer, sieve, sedimentation, and field-flow fractionation devices; however, it is not as sensitive as a good single particle counter (SPC). A good SPC device counts all the particles in a precisely known

volume, yielding the absolute concentration in various particle size classes. A SPC is sometimes employed more for its ability to measure the concentration than for its particle sizing accuracy or resolution.

The TOT method is not a suitable substitute for a good SPC for many reasons. Not all particles are counted in the TOT method. Some may be out of focus and rejected. The beam may transit across a chord and reject the particle. Finally, as will be seen below, a volume dependent on the particle size can be optically defined, and this is not as accurate as counting all the particles in a precisely known volume.

Nevertheless, if one assumes that the particles are not segregated by size as they are presented to the circling beam, then, on average, one can assume the calculated concentration is a reasonable, first-order approximation to the true concentration.

The upper limit of detection is set by the need to avoid overlapping particles which results in shifts to apparently larger sizes. Only one particle is allowed in a volume the shape of a rectangular parallelepiped. Two sides of the volume are set equal to twice the particle diameter since particles cannot get any closer than  $d_p$  apart. The long dimension is set to  $4z$ , where  $z$  is determined by the criterion that the particle diameter  $d_p = 2w(z)$ . This optically defined volume leads to the following relationship when  $d_p / 2w_0 \gg 1$ :

$$\Phi_M = \frac{I}{48 \cdot w_0}$$

Where  $\Phi_M$  is the maximum theoretical volume fraction. Thus, for particle diameters larger than about  $5\mu$ , this theoretical limit in water ( $I = I_0/n$ ) is 1.7% v/v. Measurements on  $2\mu$  fat particles in milk have been made successfully in a specially designed flow cell up to 0.42% v/v which corresponds to  $10^{+9}$  particles/cc. The path length in the cell was 1 mm, allowing the measurement of a milky looking sample. The standard path length is 10 mm. Such high concentration measurements are not possible with Fraunhofer devices, because, unlike the TOT method, the beam is not highly focused.

The above calculation for the maximum volume fraction is based on theory. It is a limiting value. Turbidity and multiple scattering, both complicated functions of concentration, particle size, and refractive indices, set the practical limit. As a first approximation for an unknown sample, a concentration of 0.2% v/v is a good starting point.

**Nonspherical Particles.** When the circling beam encounters a nonspherical particle, many of the interactions of the beam and particle will lead to asymmetric pulses which are rejected. Consider, as an extreme case, a long, thin rod *randomly* oriented as it passes, through the circling beam. Interactions perpendicular to the length of the rod will lead to acceptable pulses; the size recorded will correspond to the width of the particle. There will be fewer acceptable interactions along the length of the particle, provided the length is small compared to the circling diameter.

The result, in this extreme case, is an apparent size distribution favoring sizes close to the rod's width, with the possibility of a second mode corresponding to the length of the rod. It may be argued that the TOT technique is not suitable for such highly nonspherical particles. The argument is correct, but no more so than for any other nonimaging device, where the size obtained is always a function of the particle shape. For globular particles the TOT technique is

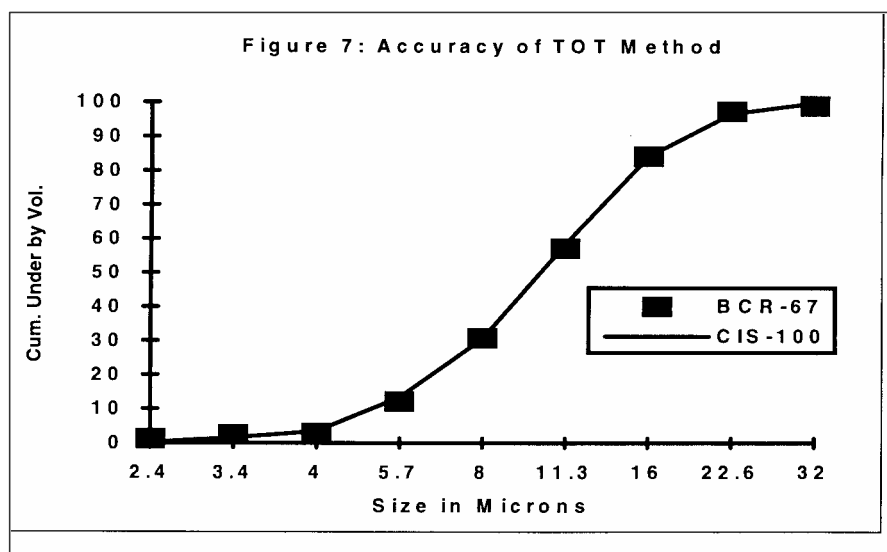
acceptable. For highly irregularly shaped particles, it is important to characterize the shape and size through image analysis. In such cases, the results obtained using the TOT method alone may not be sufficient to characterize the particle size distribution.

Interestingly, the simplicity of the TOT optical design allows images to be obtained by inserting optics at right angles to the laser beam. A synchronized flash and a CCD camera allow measurements from approximately 2  $\mu$  to 3,600  $\mu$ . Images provide not only the opportunity for particle sizing but also the opportunity to inspect the state of aggregation. An example of image analysis is given in this paper.

### Measurements and Discussion

The TOT technique has been used for about a decade to solve both routine and complex problems in particle sizing. A few have been chosen to illustrate some of the capabilities of this technique.

**Accuracy: BCR 67, Standard Quartz Powder.** The results shown in Figure 7 demonstrate the basic accuracy of the TOT method. The sample, BCR 67, is a standard quartz powder (4) with a broad size distribution from 2.4  $\mu$  to 32  $\mu$ . The sample was prepared as a suspension in water using 0.1% sodium hexametaphosphate as a wetting/dispersing agent. Approximately 2 cc were placed in a standard, plastic cuvette. During the few minutes it takes to make the measurement, the particles were kept in suspension using a magnetic stir bar. Note the good agreement between the standard values obtained from sedimentation and the TOT results.

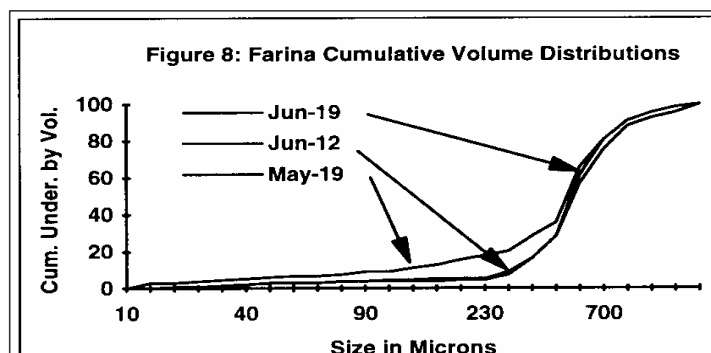


**Large, Airborne Particles: Farina (Wheat).** Farina is ground wheat, sieved in order to produce various fractions. The coarse fractions are used in making specialty foods like Cuscus, a Mediterranean delicacy. A fine fraction is used to make flour for bread. A super fine fraction is used in the production of baby foods. The production costs and selling price are functions of the particle size distribution. (Galam Ltd., Kibbutz Mahanit, Israel. Galam is a manufacturer of Farina.) Due to absorption, measurements cannot be made in liquid.

Figure 8 shows the overlap of three runs made on different dates: May 19, June 12, and June 19, 1995. The cumulative undersize distributions by volume are shown. The volume median

diameter is around 500  $\mu$  for all three, with the curve for the run on May 19 shifted to distinctly smaller sizes, indicating this sample was suitable for use as a higher priced baby food fraction.

All three samples cover a broad range of sizes from a few 10's of microns to just under 1 mm. Measurements took approximately 2 minutes using a vibrating platform, similar to a riffler, to feed randomly these free-flowing particles into a 1 cm x 1 cm flow cell. Gentle suction is applied to assist the gravity feed while making the measurements.



**Oriented Rods: Mixture of Hardwood and Softwood Fibers.** In the manufacture of paper, a mixture of hardwood (HW) and softwood (SW) fibers is used. Softwood is harder to shear, folds more easily, and is less expensive. Hardwood is easier to shear, folds less easily, and is more expensive. The proper mixture provides the desired properties at the right cost. During the milling process both HW and SW species are fed continuously into headboxes. It is desirable to adjust, in real-time, the ratio of HW to SW to get the final, desired properties.

Typical hardwoods used in paper making include the following: redgum, birch, aspen, oak, eucalyptus, and gmelina. Unprocessed, they vary in length from roughly 300 $\mu$  to 1,200 $\mu$ , and the widths vary from 15 to 30  $\mu$ . Typical softwoods used in paper making include southern yellow pine and western hemlock. Unprocessed, they vary in length from 2 to 8 mm, and the widths vary from 25 to 45  $\mu$  (5).

During processing the long fibers are chopped into a variety of lengths. Thus, the length distributions, and therefore the volume distributions, are broad and overlapping. Even though the width distributions overlap slightly, they characterize more sharply the differences between the HW and SW, because the widths remain nearly unchanged by the processing. By orienting the fibers in a flowing cell and measuring the fiber widths using the TOT method, one can reconstruct the volume distribution without ever measuring the fiber lengths.

Consider a long rod of diameter  $d_p$  and length  $L$  made to flow with speed  $V_{\perp}$  perpendicular to the tangential speed  $V_T$ . As long as both  $V_{\perp}$  and  $V_T$  are constant, and  $V_T \gg V_{\perp}$  the long rod will be cut into  $N_c$  pieces, each of length  $\Delta l$ . The volume  $V$  and length  $L$  of a rod are given by

$$V = \frac{\pi}{4} d_p^2 L \quad \text{where } L = N_c \Delta l$$

The surface area of  $N_c$  spheres, each with a diameter of  $d_p$  is given by

$$A = \mathbf{p} d_p^2 N_c$$

From these relationships one can show that the differential volume distribution is given by

$$\frac{dV}{dd} = \frac{\mathbf{p}}{4} \cdot \Delta l \cdot d_p^2 \cdot \frac{dN}{dd_p}$$

where  $N$  is equal to the sum of  $N_c$ , over all the rods. In addition, one can show that the differential surface area distribution of  $N$  total spheres with diameter  $d_p$  is given by

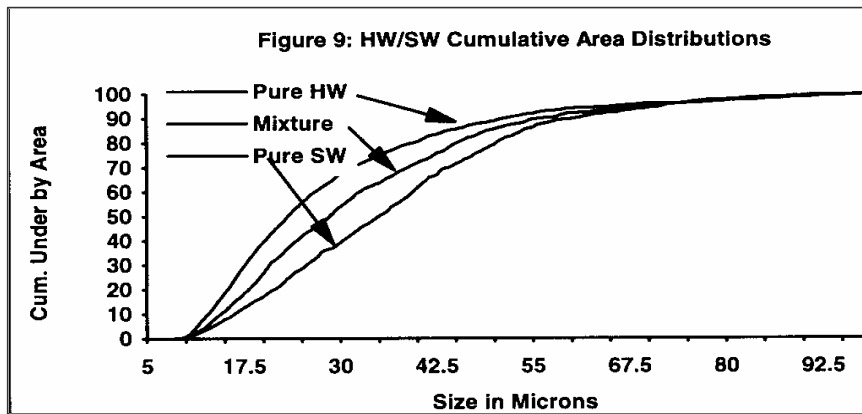
$$\frac{dA}{dd_p} = \mathbf{p} \cdot d_p^2 \cdot \frac{dN}{dd_p}$$

where it should be emphasized that this differential surface area distribution formed by cutting equal slices from oriented rods, is not the surface area distribution of the rods themselves. Combining the above result with that for the differential volume distribution yields

$$\frac{dV}{dd_p} = \frac{\Delta l}{4} \cdot \frac{dA}{dd_p}$$

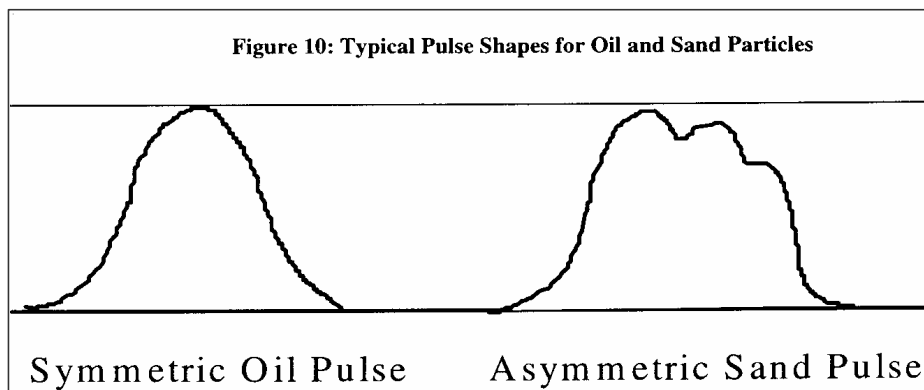
This rather interesting result says that the differential volume distribution with respect to the width of the rod is proportional to the differential surface area distribution of spheres whose diameters equal the widths of the rods. There is no need to know the rod lengths.

It turns out that the distributions obtained are not easily separable into two modes: one corresponding to the HW width and one to the SW width. However, by calibrating using a run of pure HW and pure SW, one can establish a working formula for calculating the ratio of HW:SW from the cumulative distribution obtained from a mixture. Figure 9 shows an example. Notice it is the cumulative undersize surface area distribution that is plotted as a function of particle size.



**Using Pulse Shape to Discriminate: On-line Measurements of Oil /Sand Mixtures.** Many single particle counters determine particle size by measuring the height of an electrical pulse and compare it to pulses generated using standards. In the TOT method it is the pulse width that determines particle size; calibration is not required. However, the pulse shape does play a role in deciding if the pulse is processed or not. Asymmetric pulses, pulses with long rise/fall times, and pulses with insufficient amplitude are normally rejected as corresponding to highly irregular shapes, chords, or out-of-focus particles. In special cases, with *a-priori* knowledge, asymmetric pulses are used to discriminate against two different particle types. This capability has been used to discriminate the particle size distribution of oil droplets remaining in sea water after processing in the presence of a background of sand particles.

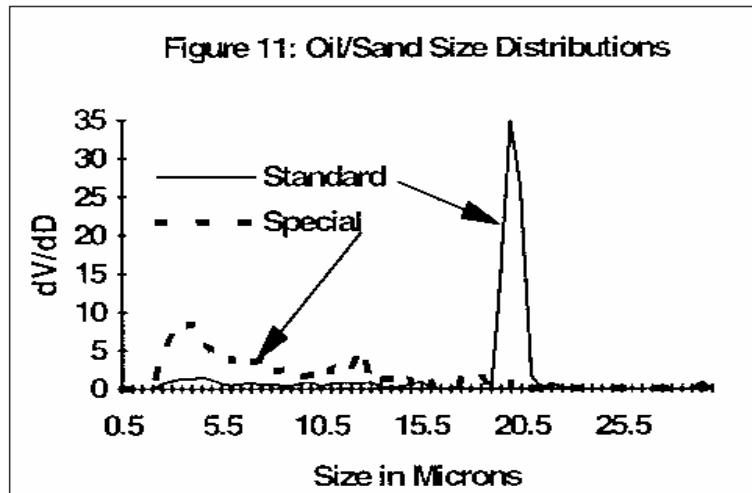
Figure 10 shows two pulses. The more symmetric pulse is typical of an opaque oil droplet in sea water, the droplets remaining after most of the oil has been separated using a combination of holding tanks and hydrocyclones (6). The less symmetric pulse is typical of sand particles. The shape of the pulse from sand is believed to arise from internal reflections that are not present in a dark, strongly absorbing oil droplet. Since the pulse widths are roughly equal, it would be impossible to discriminate oil from sand based on size alone.



An obscuration ratio is defined as the ratio of the (rise time)/(fall time). Opaque oil droplets have characteristically higher obscuration ratios at the same particle size than do sand particles, and a threshold can be established as a function of particle size. Pulses with obscurations exceeding the threshold correspond to oil droplets and are processed further to determine the particle size; pulses with obscurations less than the threshold correspond to sand particles are not processed.

Figure 11 shows the overlay of two differential volume size distributions obtained on the same sample of oil droplets in salt water spiked with 20  $\mu$  sand particles. The distribution marked Standard, with the strong peak at 20 $\mu$ , was obtained using all the pulses. The distribution marked Special, without the peak, was obtained using the threshold criterion set by the obscuration. No trace of the sand peak is evident.

These measurements have been made with both a laboratory instrument and a dedicated, on-line, flow instrument with results equal to those shown here (7).



**Dynamic Shape Analysis: Fly Ash/Cement Mixtures.** Not all problems in particle sizing can be solved by assuming a spherical shape. Sometimes the information obtained from imaging is necessary. A good example of this consists of determining the amount of fly ash in a mixture with cement. Such a mixture is used in the making of concrete for surfacing roads. Fly ash is much less expensive than concrete, yet if it constitutes more than 20% of the mixture, the final properties of the concrete suffer (8).

Figure 12 shows a few typical renderings of fly ash and cement particles. Three things are evident: there is not a significant difference in size between the two types of particles, there is not a significant difference between the aspect ratios (length/width) between the two types of particles (both are globular); but the perimeter of fly ash particles is typically smoother than the perimeter of cement particles. This difference in perimeter can be exploited using the shape factor.

The shape factor, SF, is here defined as  $4p \cdot \text{Area}/(\text{Perimeter})^2$ , where the Area and Perimeter are determined from the number and size of the pixels covering the particle and lying on the external contour. Using the definition, SF is exactly 1 for a circle, 0.785 for a square, and approaches zero for a long, thin rectangle. For smooth globular particles like Fly Ash, the SF is closer to 1 than for jagged-perimeter particles like cement with their longer perimeters.

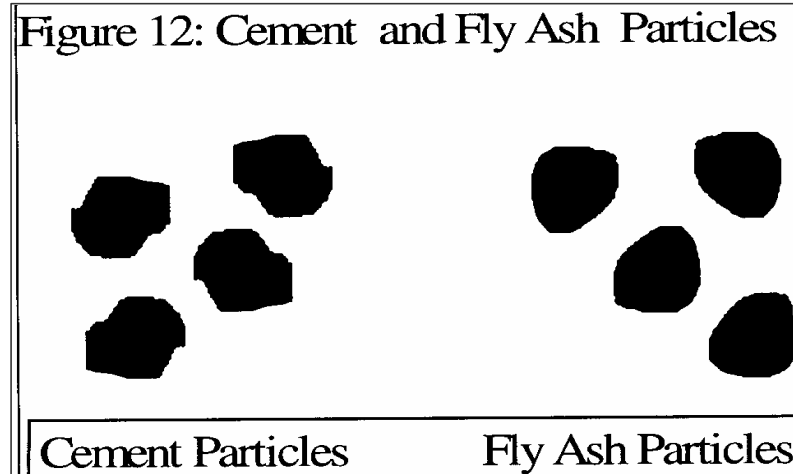
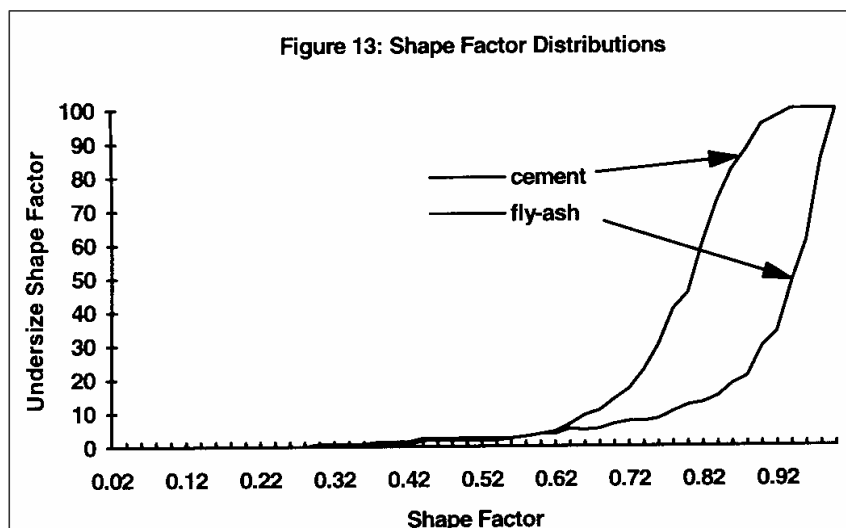


Figure 13 shows the cumulative SF distributions for cement and fly ash separately. As expected, the shape factors for cement are smaller, with approximately 100% less than 0.90. From the cumulative SF curve corresponding to the mixture, the amount of cement is set empirically as the percent corresponding to a SF of 0.90. Mixtures corresponding to less than 80% cement are rejected.



It should be noted that the images formed were obtained from particles falling through the measurement zone. As such, the images formed are dynamic, two dimensional images. This is different than forming the image from particles that have fallen onto a microscope slide.(an alternate method possible for this instrument). For example, the stable position of platelet particles on a slide is face up, not standing on an edge. When analyzed, this static image will produce larger equivalent spherical sizes compared to an analysis of moving particles. Dynamic image analysis, also called dynamic shape characterization, offers the possibility of averaging size/shape information more realistically than traditional static image analysis. However, to date, there are no definitive studies on the differences. This remains a challenge for future investigation.

## Summary

The TOT method presents an interesting blend of characteristics with the following disadvantages:

- It is relatively slow on broad distributions;
- Limited to particle sizes greater than  $\sim 0.5 \mu$ ;
- Requires care in presenting large, dense particles in the measuring zone to avoid bias;

and the following advantages:

- Relatively high resolution from measurements on single particles;
- Straight forward data analysis;
- Can be made to operate over a wide size range;
- Very versatile, operating on particles in liquids, in air, or on transparent slides;
- Easily coupled to image analyzer, allowing size/shape analysis and visualization of shape and the state of aggregation.

Its unique capability of using pulse shape and height to ensure accuracy or to discriminate one type of particle from another, and pulse widths to determine particle size, make the TOT technique capable of solving some difficult, yet practical and interesting, particle sizing problems.

## Literature Cited

1. Aharonson; Karasikov, N.; *J. Aerosol Science*, **1986**, 17, 530-536.
2. Karasikov, N.; Krauss, M.; Barazani, G.; In *Particle Size Analysis*; Lloyd, P.J Ed.; John Wiley & Sons: New York **1988**.
3. Melles-Griot Optics Catalogue; Melles-Griot: Irvine, California, **1995-1996**, 2-7.
4. BCR standard samples are available from the Commission of the European Communities, Community Bureau of Reference (BCR), Directorate General XII, 200 Rue de la Loi, B 1049 Brussels, Belgium.
5. Kocurek, M.J.; Stevens, C.F.B.; In *Pulp and Paper Manufacture*; TAPPI: Atlanta, Georgia, 1989, Vol. 1.
6. Davies, R.H.S.; Palmer, A.J.; "Use of Hydrocyclones for Solids Separation and Cleaning Applications", Presented at *4th International Conference on Water Management Offshore*, Aberdeen, Scotland, **1995**.
7. Tulloch, S.J.; "Evaluation of On-line Oil-in-Water Monitors and Particle Size Analysis In Relation to the Concentration and Drop Size Measurement of Dispersed Oil Droplets", *Project No. OWTC1901059*; Orkney Water Test Center Ltd.: Orkney, U.K.
8. Gaskin, R.; *Laboratory Practice U.K.*, **1991**, 39.

Reprinted from Symposium Series 693  
Particle Size Distribution III  
Theodore Provder, Editor  
Published 1998 by the American Chemical Society

